Preprints (www.preprints.org) | NOT PEER-REVIEWED | Posted: 20 October 2022

doi:10.20944/preprints202210.0314.v1

Article.

Evaluation of Different Cannulation Strategies for Aortic Arch Surgery Using a Cardiovascular Numerical Simulator.

Beatrice De Lazzari [1*], Massimo Capoccia [2, 3], Roberto Badagliacca [4], Claudio De Lazzari [5, 6]

[1] "Foro Italico" 4th University of Rome, Italy; beatrice.delazzari@gmail.com
[2] Leeds General Infirmary, Leeds Teaching Hospitals NHS Trust, Leeds, UK; capoccia@doctors.org.uk
[3] Department of Biomedical Engineering, University of Strathclyde, Glasgow, UK
[4] Department of Clinical, Internal Anesthesiology and Cardiovascular Sciences, "Sapienza" University of Rome, Italy; silvia.papa@uniroma1.it; roberto.badagliacca@uniroma1.it; dario.vizza@gmail.com
[5] National Research Council, Institute of Clinical Physiology (IFC-CNR), Rome, Italy
[6] Teaching University Geomedi, Tbilisi, Georgia; claudio.delazzari@ifc.cnr.it
* Correspondence: beatrice.delazzari@gmail.com

Abstract: Aortic disease has a significant impact on quality of life. Involvement of the aortic arch requires preservation of blood supply to the brain during surgery. Deep hypothermic circulatory arrest is an established technique for this purpose although neurological injury remains high. Additional techniques have been used to reduce the risk although controversy still remains. A three-way cannulation approach, including both carotid arteries and the femoral artery or the ascending aorta, has been used successfully for aortic arch replacement and redo procedures. We have developed circuits of the circulation to simulate blood flow during this type of cannulation set up. The aim is to analyse using CARDIOSIM© cardiovascular simulation platform, how the haemodynamic and energetic parameters are affected and the benefit derived with particular reference to the cerebral circulation.

Keywords: Aortic surgery; Aortic arch; Three-way cannulation approach; Carotid artery perfusion; Pressure-volume loop; Lumped parameter model; Software simulation; Cardiovascular modelling.

1. Introduction

Aortic disease has a significant impact on quality of life. Aneurysmatic dilatation and acute aortic dissection involving the aortic arch are the most devastating manifestation of aortic disease. Surgical or endovascular treatments for these conditions are currently available options. The outcome following successful total arch repair is satisfactory, but it still carries the risk of potentially devastating perioperative complications. Conventional aortic arch replacement can be offered to the majority of patients, although hybrid and endovascular techniques have gained popularity. Nevertheless, a less invasive approach can often be as technically challenging as open surgery with stroke and endo-leaks as early limiting factors and less favourable mid- to long-term outcome [1]. Mid-term outcomes and intra-operative complication rates with both hybrid and conventional aortic arch surgery remain heterogeneous and depend on centre experience and patient suitability [2]. Open repair with the elephant trunk technique [3] under hypothermic circulatory arrest is widely used with satisfactory long-term outcome [4]-[5]. More recently, the frozen elephant trunk technique using the Thoraflex™ (Vascutek, Terumo, Inchinnan,

© 2022 by the author(s). Distributed under a Creative Commons CC BY license.

Preprints (www.preprints.org) | NOT PEER-REVIEWED | Posted: 20 October 2022 doi:10.20944/preprints202210.0314.v1

Glasgow, UK) or the E-vita OPEN PLUS (JOTEC, Hechingen, Germany) hybrid device has become a popular choice which allows subsequent endovascular procedures [6]-[7]. Hybrid repair involves different techniques to debranch the aortic arch and create a suitable landing zone for an additional or staged endovascular procedure. Although aortic arch surgery has progressed significantly since the early attempts, [8]-[9], cerebral protection remains a matter of debate. Due to reduced oxygen demand and cerebral metabolism, profound hypothermia (18°C) with total circulatory arrest as the only mode of protection has been widely accepted [10] although at the expense of some neurological injury as the metabolism is never reduced to zero [11]. The use of retrograde cerebral perfusion as additional protective measure [12] has been challenged by its unpredictable effects and ability to provide adequate cerebral capillary perfusion [13]-[17]. Although retrograde cerebral perfusion is still used by some groups [18]-[19], antegrade selective cerebral perfusion has gained wide acceptance and popularity [20]-[22]. The combination of antegrade selective cerebral perfusion with moderate hypothermia [20], [23] has reduced the potential for neurological injury and allowed more time for repair [24]-[26]. Controversy remains whether unilateral or bilateral perfusion should be more appropriate [27]-[29] in the presence of completeness of the circle of Willis [30]. The "branch-first" technique without circulatory arrest or deep hypothermia has also been proposed [31]-[32].

The surgical approach consists of techniques involving different cannulation sites. When central aortic cannulation is not feasible, arterial cannulation through one of the femoral arteries (either directly or via an end-to-side Dacron graft) is appropriate. Axillary artery cannulation [33] is gaining interest, but it is not without other risks and complications [1], [34]. The innominate [35] and the common carotid artery [36] have also been considered as cannulation sites. A three-way cannulation approach, which can be used for complex and redo surgery in particular, has been recently proposed [37].

We have developed circuits of the circulation to simulate blood flow during different cannulation configurations including both common carotid arteries and either the femoral artery or the ascending aorta. CARDIOSIM© was the numerical simulator platform used for this purpose [38]. The aim was to analyse how the haemodynamic and energetic parameters were affected and the benefit derived with particular reference to the cerebral circulation.

2. Materials and Methods

2.1. Cannulation strategies for aortic arch surgery

Figure 1 shows four different cannulation strategies for aortic arch surgery as the main subject of this study. The centrifugal pump draws blood and ejects it according to the following connections:

- Right atrial (RA) cannulation to ascending aorta (AA) and bilateral common carotid artery (CC) return (top left panel), RA➔AA&CC.
- Right atrial cannulation to right femoral artery (FA) and bilateral common carotid artery return (top right panel), RA➔FA&CC.
- Right femoral vein (FV) and superior vena cava (SVC) cannulation to right femoral artery and bilateral common carotid artery return (bottom left panel), FV&SVC➔FA&CC.
- Right femoral vein cannulation to right femoral artery and bilateral common carotid artery return (bottom right panel), FV➔FA&CC.

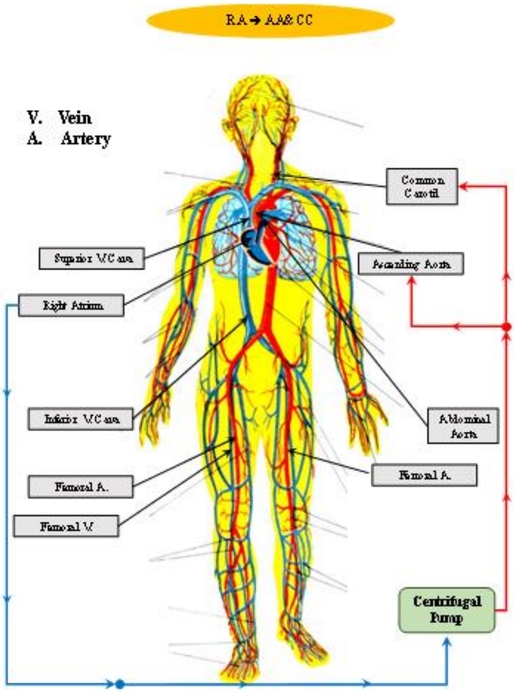
RA ➔ AA& CC
V. Vein
A. Artery
Common Carotid
Superior V.Cava
Ascending Aorta
Right Atrium
Inferior V.Cava
Abdominal Aorta
Femoral A.
Femoral A.
Femoral V.
Centrifugal Pump

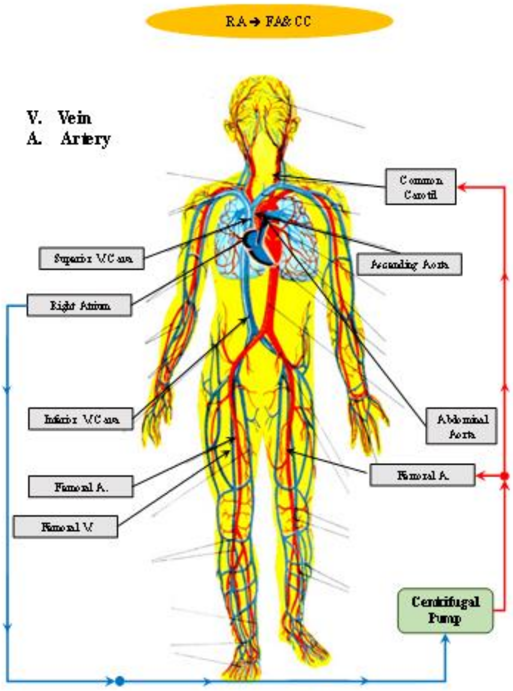
RA ➔ FA& CC
V. Vein
A. Artery
Common Carotid
Superior V.Cava
Ascending Aorta
Right Atrium
Inferior V.Cava
Abdominal Aorta
Femoral A.
Femoral A.
Femoral V.
Centrifugal Pump

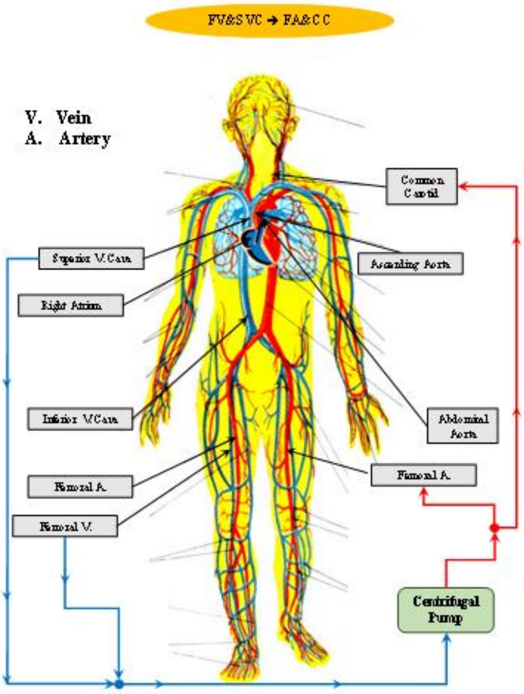
FV&SVC ➔ FA&CC
V. Vein
A. Artery
Common Carotid
Superior V.Cava
Ascending Aorta
Right Atrium
Inferior V.Cava
Abdominal Aorta
Femoral A.
Femoral A.
Femoral V.
Centrifugal Pump

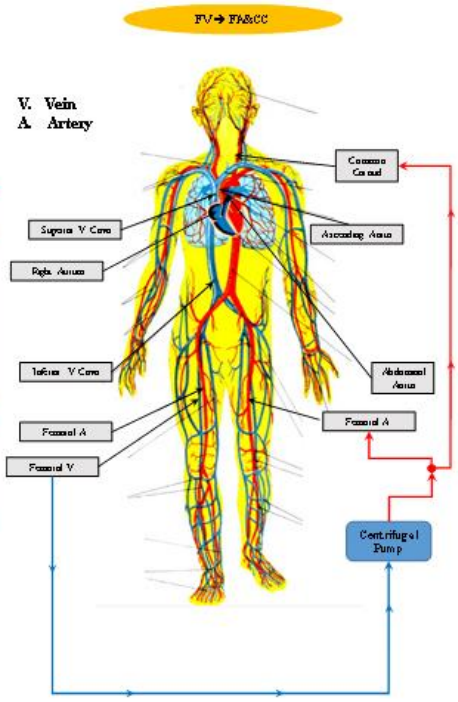
FV ➔ FA&CC
V. Vein
A. Artery
Common Carotid
Superior V Cava
Ascending Aorta
Right Atrium
Inferior V Cava
Abdominal Aorta
Femoral A
Femoral A
Femoral V
Centrifugal Pump

Figure 1. Schematic representation of the four cannulation strategies: right atrial to ascending aorta and bilateral common carotid artery return (top left); right atrial to femoral artery and bilateral common carotid artery return (top right), femoral vein and SVC to femoral artery and bilateral common carotid artery return (bottom left), femoral vein to femoral artery and bilateral common carotid artery return (bottom right).

2.2. The heart and circulatory numerical network

"In silico" study of cannulation for aortic arch surgery was performed developing new 0-D numerical modules of the cardiovascular network implemented in CARDIOSIM© platform [38]-[44]. These modules allow the reproduction of the behaviour of: native left and right ventricles; atria and septum; coronary circulation; ascending aorta and aortic arch; descending thoracic and abdominal aorta; upper limbs and head section; superior, inferior and abdominal vena cava section; renal and hepatic section; splanchnic and lower limbs sections; pulmonary circulation. Figure 2a shows an overview of the whole cardiovascular network. The native left and right ventricles, atria and septum and the ventricular, atrial and septal activity synchronized with the electrocardiographic (ECG) signal are implemented using the time-varying elastance concept [40],[41],[43],[44]. This numerical representation allows the simulation of inter-ventricular and intra-ventricular dyssynchrony. Specific modules of the coronary circulation are available in CARDIOSIM© platform [38]. The module of the coronary circulation presented in [45] was selected for this study. Figure 2a shows two different electric analogues used to reproduce the behavior of the aortic (AV), mitral (MV), tricuspid (TV) and pulmonary (PV) valves [38]. A representation with an ideal diode was chosen for this study: when the pressure across the valve was positive, the valve opened and allowed blood flow; when the pressure was less than or equal to zero, the valve closed and blood flow was zero. The whole pulmonary circulation was modelled as described in current literature [43], [44], [46], [47].

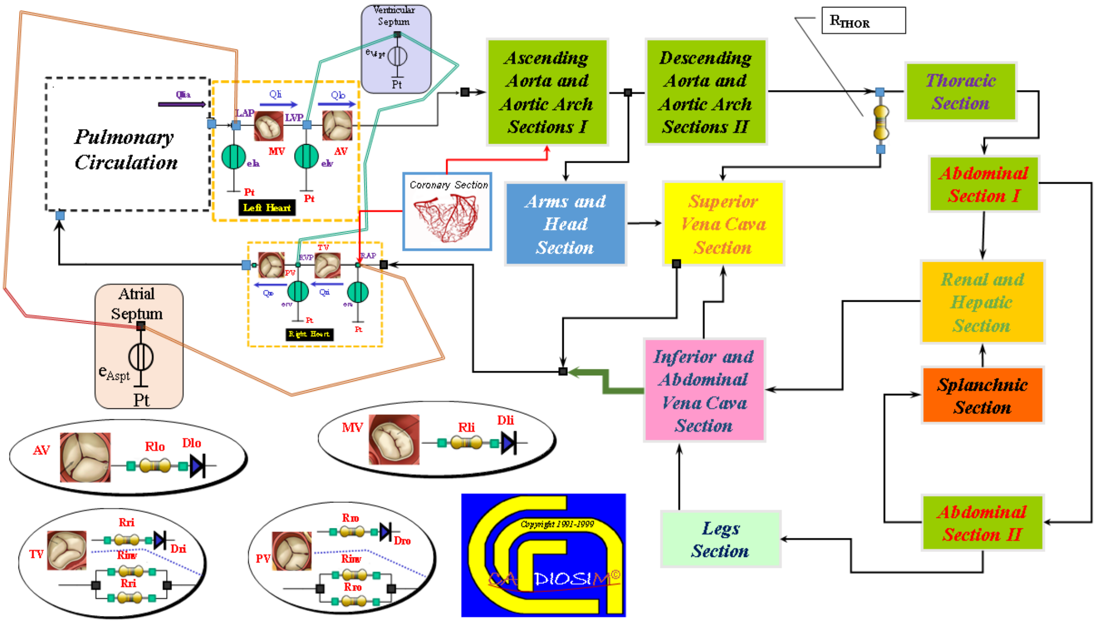

Figure 2. **a** Schematic representation of the cardiovascular system implemented in CARDIOSIM© software platform.

Figure 2b shows the electric analogue of the following compartments: ascending and descending aorta, aortic arch and abdominal tract. All these sections are modelled with resistance, inertance and compliance (RLC) elements. The thoracic compartment is modelled with two resistances (R_{THOR} and R_{ATI}), inertance (L_{ATI}) and compliance (C_{ATI}). The abdominal section is divided in two compartments both electrically represented with RLC

Preprints (www.preprints.org) | NOT PEER-REVIEWED | Posted: 20 October 2022 doi:10.20944/preprints202210.0314.v1

elements. Finally, the behavior of the superior vena cava section is reproduced with RC elements. The symbols used in Figure 2b are listed in Table 1.

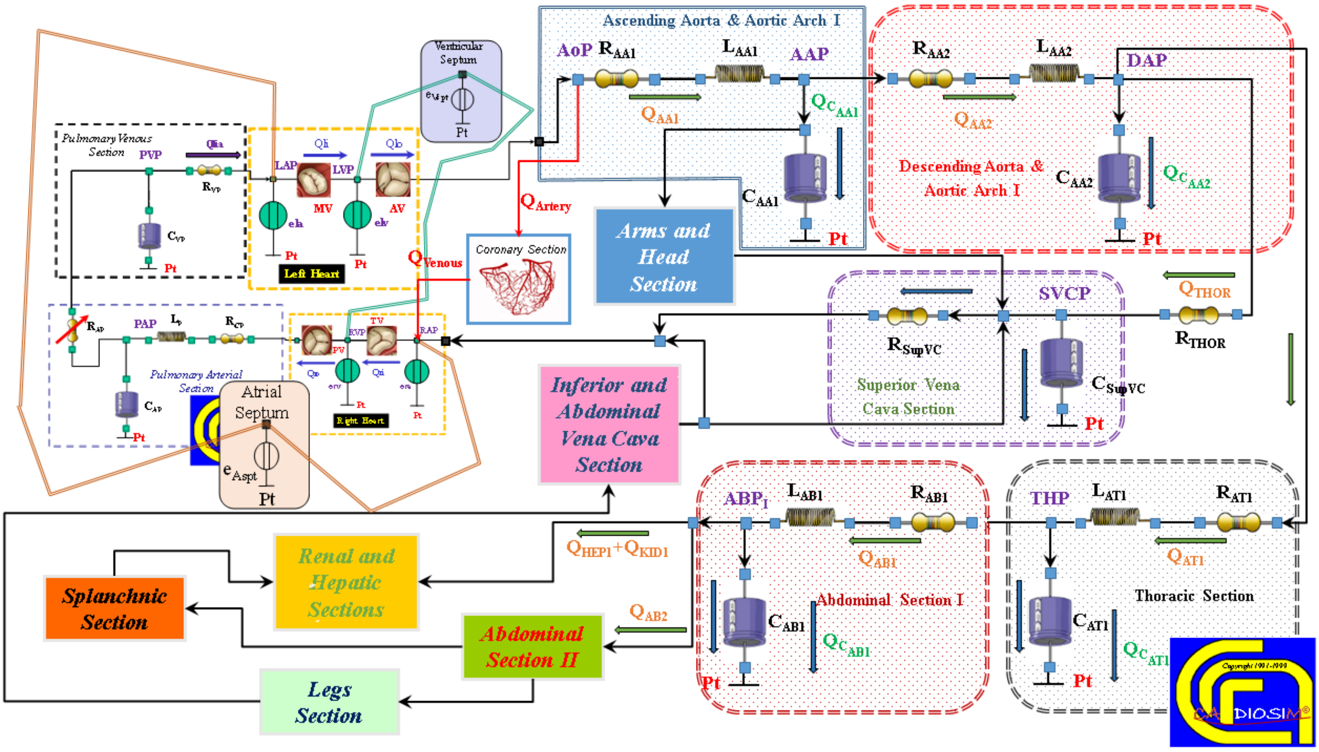

Figure 2. **b** Electric analogue of the ascending and descending aorta, aortic arch, thoracic and abdominal sections and superior vena cava.

Table 1

Symbol	Description	Unit
AoP [AAP]	Aortic [ascending and aortic] pressure	mmHg
LAP [RAP]	Left [right] atrial pressure	mmHg
LVP [RVP]	Left (right) ventricular pressure	mmHg
DAP [SVCP]	Descending aortic [superior vena cava] pressure	mmHg
THP [ABP$_I$]	Thoracic [abdominal] pressure	mmHg
HDP [ARP]	Brain [Arm] pressure	mmHg
LLEP [RLEP]	Left (right) leg pressure	mmHg
Pt	Intrathoracic pressure	mmHg
P_B	Breathing pressure	mmHg
SP [ABP$_{II}$]	Splanchnic (abdominal II) pressure	mmHg
HP [KP]	Hepatic (renal) pressure	mmHg
IVCP	Inferior vena cava pressure	mmHg
R_{AA1} [R_{AA2}]	Ascending [descending] and aortic arch resistance	mmHg·cm^{-3}·sec
L_{AA1} [L_{AA2}]	Ascending [descending] and aortic arch inertance	mmHg·cm^{-3}·sec^2
C_{AA1} [C_{AA2}]	Ascending [descending] and aortic arch compliance	mmHg^{-1}·cm^{-3}

R_{THOR} [R_{SupVC}]	Thoracic [superior vena cava] resistance	$mmHg \cdot cm^{-3} \cdot sec$
C_{SupVC}	Superior vena cava compliance	$mmHg^{-1} \cdot cm^{-3}$
R_{AT1} [R_{AB1}]	Thoracic [abdominal] resistance	$mmHg \cdot cm^{-3} \cdot sec$
L_{AT1} [L_{AB1}]	Thoracic [abdominal] inertance	$mmHg \cdot cm^{-3} \cdot sec^{2}$
C_{AT1} [C_{AB1}]	Thoracic [abdominal] compliance	$mmHg^{-1} \cdot cm^{-3}$
R_{LFA} [R_{LFV}]	Left femoral arterial [venous] resistance	$mmHg \cdot cm^{-3} \cdot sec$
R_{RFA} [R_{RFV}]	Right femoral arterial [venous] resistance	$mmHg \cdot cm^{-3} \cdot sec$
C_{LLE} [C_{RLE}]	Left [right] femoral compliance	$mmHg^{-1} \cdot cm^{-3}$
R_{ARM1} and R_{ARM2} [C_{ARM}]	Upper limb resistances [compliance]	$mmHg \cdot cm^{-3} \cdot sec$ [$mmHg^{-1} \cdot cm^{-3}$]
R_{HD1} and R_{HD2} [C_{HD}]	Brain resistances [compliance]	$mmHg \cdot cm^{-3} \cdot sec$ [$mmHg^{-1} \cdot cm^{-3}$]
R_{infVC1} and R_{infVC2} [C_{InfVC}]	Inferior vena cava resistances (compliance)	$mmHg \cdot cm^{-3} \cdot sec$ [$mmHg^{-1} \cdot cm^{-3}$]
R_{HEP1} and R_{HEP2} [C_{HEP}]	Hepatic resistances (compliance)	$mmHg \cdot cm^{-3} \cdot sec$ [$mmHg^{-1} \cdot cm^{-3}$]
R_{KID1} and R_{KID2} [C_{KID}]	Renal resistances (compliance)	$mmHg \cdot cm^{-3} \cdot sec$ [$mmHg^{-1} \cdot cm^{-3}$]
R_{SP1} and R_{SP2} [C_{SP}]	Splanchninc resistances (compliance)	$mmHg \cdot cm^{-3} \cdot sec$ [$mmHg^{-1} \cdot cm^{-3}$]
R_{ABII} [C_{ABII}]	Abdominal (II) resistance (compliance)	$mmHg \cdot cm^{-3} \cdot sec$ [$mmHg^{-1} \cdot cm^{-3}$]
L_{ABII}	Abdominal (II) inertance	$mmHg \cdot cm^{-3} \cdot sec^{2}$
R_{AbdVC} [C_{AbdVC}]	Abdominal vena cava resistance (compliance)	$mmHg \cdot cm^{-3} \cdot sec$ [$mmHg^{-1} \cdot cm^{-3}$]
Ees_{Left} [Ees_{Right}]	Left (right) ventricular end-systolic elastance	mmHg/ml
Eas [Ea_{P}]	Systemic (pulmonary) arterial elastance	mmHg/ml
Eas/Ees_{Left} [Ees_{Right}/Ea_{P}]	Left (right) ventricular-arterial coupling	-----

The circuit representation of the upper and lower limbs and the head sections with the four different cannulation strategy implemented in CARDIOSIM© are illustrated in Figure 2c. The nomenclature of the symbols is listed in Table 1. The lower limb section consists of two parts reproducing left and right limb circulation. The left (right) arterial circulation of the lower limb is modelled with a variable resistance R_{LFA} (R_{RFA}), the resistance R_{LFV} (R_{RFV}) reproduces the venous circulation and the capacitor C_{LLE} (C_{RLE}) represents the left (right) compliance. The upper limbs are modelled with two resistances R_{ARM1} (variable resistance) and R_{ARM2} reproducing arterial and venous circulation respectively and compliance C_{ARM}. The arterial and venous cerebral circulation is reproduced with a variable resistance R_{HD1} and a resistance R_{HD}, respectively; the capacitor C_{HD} mimics the vessel compliance.

Figure 2d shows the electrical analogue of the second abdominal tract modelled with RLC elements. The variable resistance R_{SP1} and the resistance R_{SP2} allow the simulation of the arterial and the venous circulation of the splanchnic tract; the capacitor C_{SP} mimics its compliance.

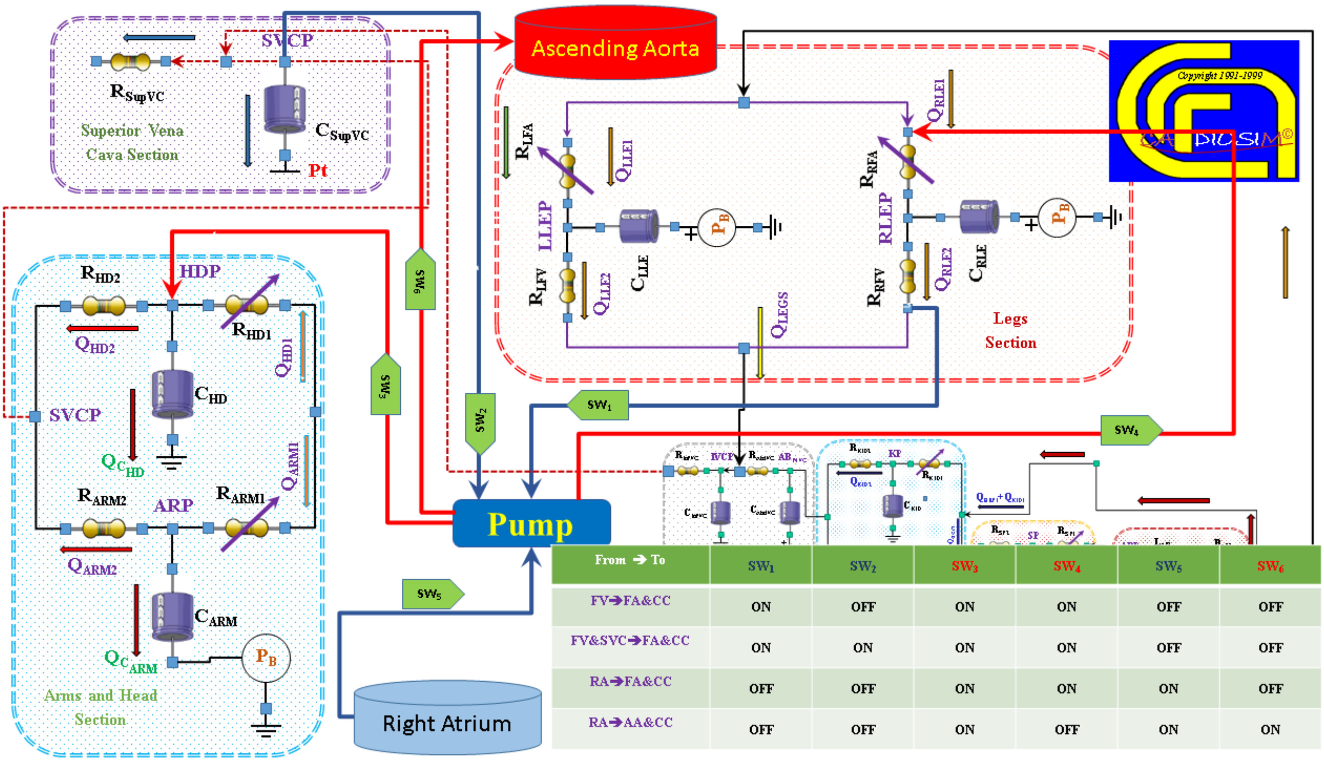

From ➔ To	SW₁	SW₂	SW₃	SW₄	SW₅	SW₆
FV➔FA&CC	ON	OFF	ON	ON	OFF	OFF
FV&SVC➔FA&CC	ON	ON	ON	ON	OFF	OFF
RA➔FA&CC	OFF	OFF	ON	ON	ON	OFF
RA➔AA&CC	OFF	OFF	ON	OFF	ON	ON

Figure 2. **c** Electric analogue of the upper and lower limbs and the head. The six switches allow the activation of one of the four cannulation strategies.

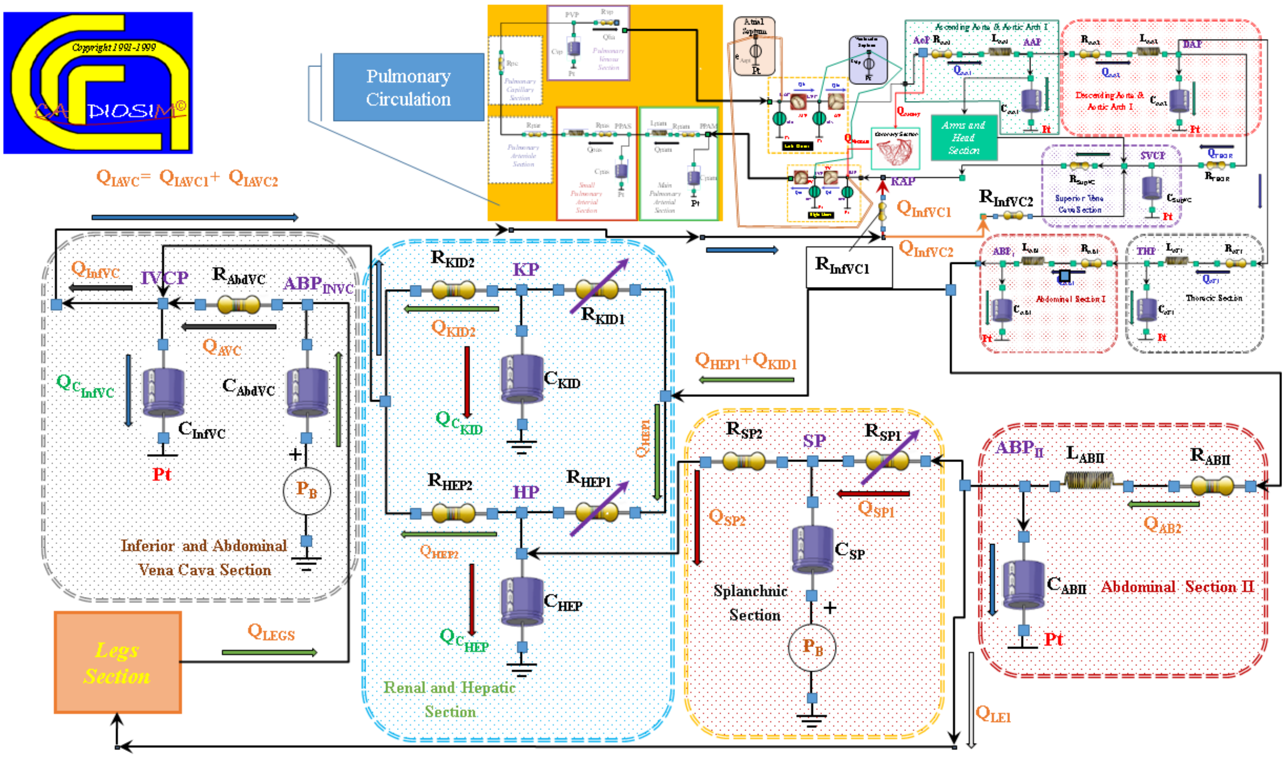

Figure 2. d Electric analogue of abdominal section (II), splanchnic, renal, hepatic, inferior and abdominal vena cava sections.

Preprints (www.preprints.org) | NOT PEER-REVIEWED | Posted: 20 October 2022 doi:10.20944/preprints202210.0314.v1

The behaviour of the arterial and venous renal (hepatic) section is simulated with a variable resistance R_{KID1} (R_{HEP1}) and the resistance R_{KID2} (R_{HEP2}), respectively. The compliance of the renal and hepatic vessels is modelled with the capacitors C_{KID} and C_{HEP}, respectively.

2.3. Numerical models of the cannulae and centrifugal pump

Figure 2c shows the four different cannulation strategies implemented in CARDIOSIM© platform. In the first one, the centrifugal pump draws blood from RA and ejects it in the ascending aorta and in the common carotid artery bilaterally (RA➔AA&CC). In this case the switches SW5 (which opens the input cannula connected to the right atrium), SW3 (which opens the output cannula connected to the common carotid artery) and SW6 (which opens the output cannula connected to the ascending aorta) are ON and the other switches are OFF. When the second type of cannulation is activated, the centrifugal pump draws blood from the right atrium and ejects it in the FA and in the common carotid artery bilaterally (RA➔FA&CC). This connection is obtained by switching SW5, SW3 and SW4 (which opens the output cannula connected to the femoral artery) ON and setting SW1, SW2 and SW6 OFF. In the connection (FV➔FA&CC), the pump draws blood from the femoral vein and ejects it in FA and CC. The cannulation can be configured by setting SW1 (which opens the input cannula connected to the femoral vein), SW3 and SW4 ON. Finally, in the last connection, the centrifugal pump draws blood from FV and the superior vena cava and ejects it in FA and CC. The cannulation (FV&SVC➔FA&CC) can be activated by switching SW1, SW2 (which opens the input cannula connected to SVC), SW3 and SW4 ON whilst SW5 and SW6 are switched OFF. All the cannulae are modelled with RLC elements [43].

The numerical model of the centrifugal pump implemented in CARDIOSIM© has been previously described in [43],[48].

2.4. Simulation Protocol

The results of the simulations performed in this work were obtained starting from basal conditions and setting heart rate (HR), left and right ventricular and septal elastance, arterial and venous resistances and compliances for all compartments to achieve minimal physiological conditions characterized by HR=90 beat/min, systolic aortic pressure (AoP_{sys})=90 mmHg, LAP=21 mmHg, RAP=10 mmHg, PAP=18 mmHg, CO=4.3 l/min. Starting from basal conditions, each cannulation configuration was activated by setting the centrifugal pump speed to 2000, 2500, 3000, 3500, 4000 and 4500 rpm. The effects induced by different cannulations on the left and right ventricular loop and on the left atrial loop are presented and discussed. Furthermore, the instantaneous waveform of the aortic and pulmonary arterial pressures for each cannulation configuration is included in the result section. Finally, an analysis of the percentage variations of the haemodynamic and energetic variables calculated with respect to basal conditions for each cannulation configuration and different speeds of the centrifugal pump was carried out in this study. Haemodynamic variables such as mean aortic pressure, PAP, LPA, RAP, CO, left (right) ventricular-arterial coupling Ea_S/Ees_{Left} (Ees_{Right}/Ea_P), cerebral, renal and superior vena cava flow together with energetic variables such as left and right ventricular external work (EW) and right ventricular pressure volume area (PVA) were analysed.

3. Results

Figure 3 shows the effects induced on the left (top left panel) and right (bottom left panel) pressure-volume loops by different rotational speed of the centrifugal pump applied when the cannulae are connected in RA➔FA&CC mode. The right panel of the figure shows the right atrial to femoral artery and bilateral common carotid artery cannulation. The different left and right ventricular loops were obtained in basal conditions (black dashed line) and when the rotational pump speed was set to 2000, 2500, 3000, 3500, 4000

Preprints (www.preprints.org) | NOT PEER-REVIEWED | Posted: 20 October 2022 doi:10.20944/preprints202210.0314.v1

and 4500 rpm. When the rotational pump speed increased, the left (right) ventricular loop shifted to the left (right) with a decrease (increase) in left (right) ventricular end-diastolic (EDV) and end-systolic (ESV) volume.

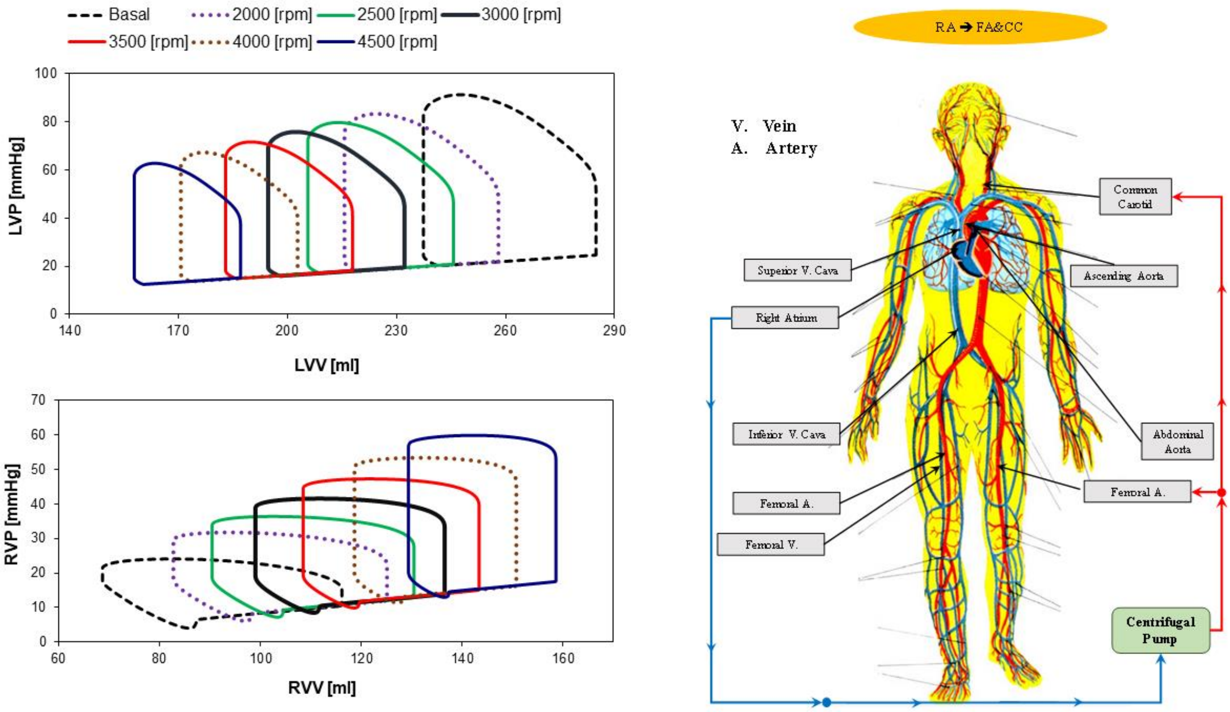

Figure 3. Top (bottom) left panel shows the left (right) ventricular pressure-volume loops in basal conditions (dashed black line) and for RA➔FA&CC cannulation with centrifugal speed pump set to 2000 rpm (dashed lilac line), 2500 rpm (green line), 3000 rpm (continuous black line), 3500 rpm (red line), 4000 rpm (dashed brown line) and 4500 rpm (lilac line). The ventricular loops obtained using CARDIOSIM© were stored in excel files and subsequently plotted. The right panel shows the RA➔FA&CC cannulation in which the centrifugal pump draws blood from the right ventricle and ejects it in the femoral artery and common carotid artery bilaterally.

Figure 4 shows the comparison of the four different methods of cannulation obtained setting the rotational pump speed to 2000 rpm. Left ventricular pressure-volume loops obtained using the software simulator were stored in excel files and subsequently plotted. The top panel shows the left ventricular pressure-volume loop in basal conditions (dashed black line) following RA➔AA&CC cannulation, obtained connecting the input cannula to the right atrium and the output cannulae to the ascending aorta and common carotid artery bilaterally (red line); RA➔FA&CC cannulation (green line); FV➔FA&CC cannulation, obtained connecting the input cannula to the femoral vein and the output cannulae to the femoral artery and common carotid artery bilaterally (blue line) and FV&SVC➔FA&CC cannulation, obtained connecting the input cannulae to the femoral vein and the superior vena cava and the output cannulae to the femoral artery and common carotid artery bilaterally (lilac line). The middle (bottom) panel shows the left atrial (right ventricular) pressure-volume loops.

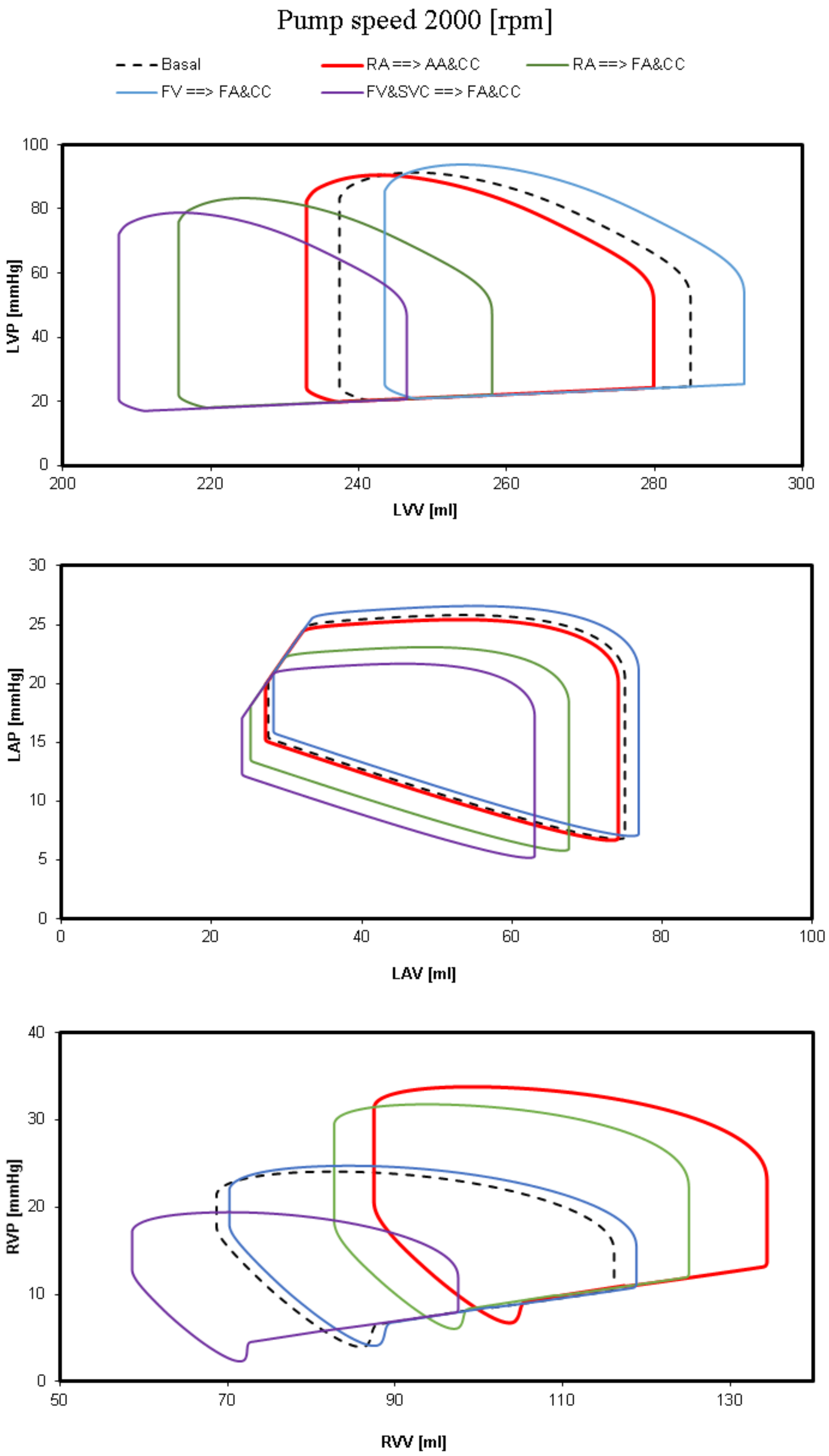

Figure 4. The top (middle) panel shows the left ventricular (atrial) pressure volume loop obtained in basal conditions and following the four different methods of cannulation when the centrifugal pump speed was set to 2000 rpm. The bottom panel shows the right ventricular pressure-volume loops. The dashed black loop is obtained in basal conditions. The red, green, light blue and lilac loops are obtained following RA➔>AA&CC, RA➔FA&CC, FV➔FA&CC and FV&SVC➔FA&CC connection, respectively. .

Preprints (www.preprints.org) | NOT PEER-REVIEWED | Posted: 20 October 2022 doi:10.20944/preprints202210.0314.v1

Figure 5. shows the aortic pressure (AoP) and pulmonary arterial pressure (PAP) waveforms simulated in basal conditions and following FV&SVC➔FA&CC cannulation with pump rotational speed set to 2000, 3500 and 4500 rpm.

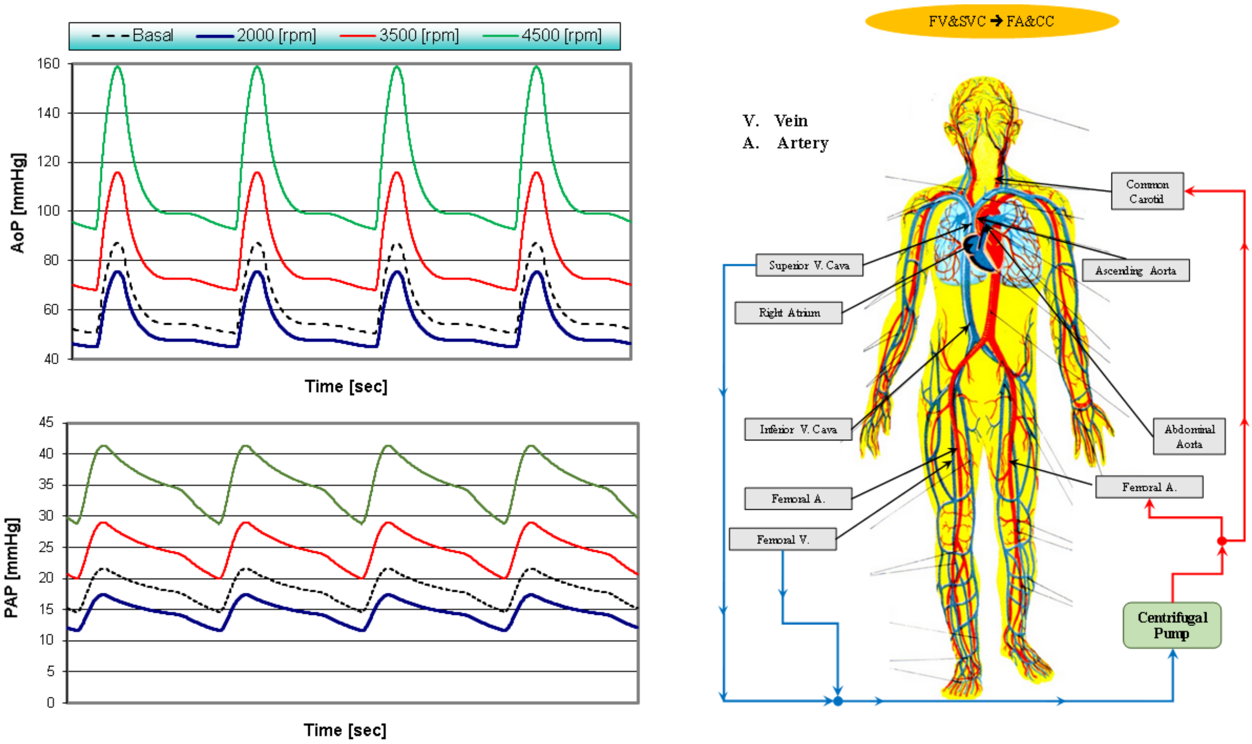

Figure 5. AoP (top left panel) and PAP (bottom left panel) waveforms obtained in basal conditions and with FV&SVC➔FA&CC cannulation when the pump rotational speed was set to 2000, 3500 and 4500 rpm. The right panel shows the FV&SVC➔FA&CC cannulation in which the centrifugal pump has two input cannulae (from superior vena cava and femoral vein) and two output cannulae (to femoral and common carotid arteries).

When the pump speed was set to 2000 rpm, the AoP and PAP waveforms (blue) moved downward compared to basal conditions.

Figure 6 shows the effects induced on the right ventricular pressure-volume loop (top left panel) and instantaneous PAP waveform (bottom left panel) by FV➔FA&CC cannulation when the rotational pump speed was set to 2000, 2500, 3000 and 3500 rpm. This type of cannulation generated limited effects compared to basal conditions (black dashed line) when the centrifugal pump speed was set to 2000 rpm (red line). When the pump rotational speed increased, the right ventricular pressure volume loop shifted to the right increasing both ESV and EDV. Instantaneous PAP waveforms were also affected by high pump rotational speeds.

Preprints (www.preprints.org) | NOT PEER-REVIEWED | Posted: 20 October 2022 doi:10.20944/preprints202210.0314.v1

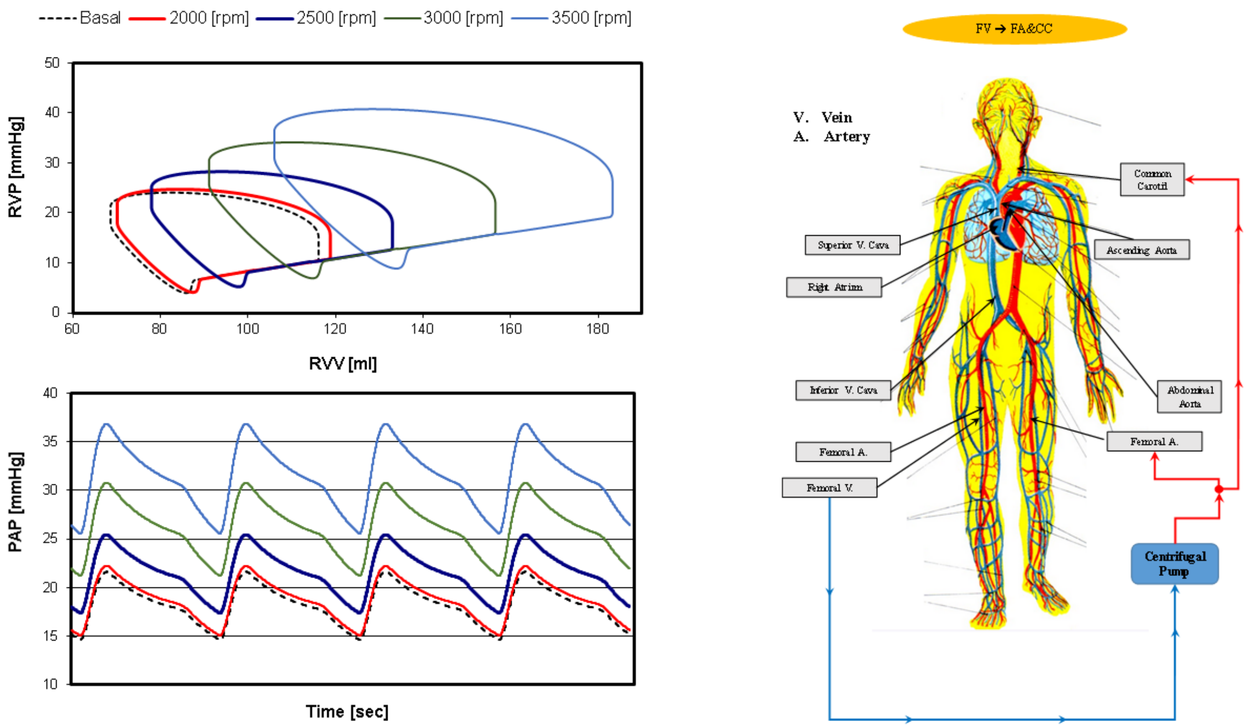

Figure 6. Right ventricular pressure-volume loops (top left panel) and instantaneous PAP waveforms (bottom left panel) obtained in basal conditions (black dashed line) and with FV➔FA&CC cannulation when the pump rotational speed was set to 2000 (red line), 2500 (blue line), 3000 (green line) and 3500 (light blue line) rpm. The ventricular loops and the instantaneous waveforms obtained using CARDIOSIM© were stored in excel files and subsequently plotted. In FV➔FA&CC cannulation (right panel), the centrifugal pump draws blood from the femoral vein and ejects it in the femoral artery and common carotid artery bilaterally.

The outcome of RA➔AA&CC cannulation on the left atrial pressure-volume loop and on the aortic pressure (AoP) is shown in Figure 7. This type of cannulation produced negligible effects when the speed of the pump was set to 2000 rpm (red lines in the top and bottom left panels). At higher pump speeds, the loops (top left panel) move to the right for high values of the left atrial end-diastolic volume. AoP increased considerably when the pump rotational speed was set to 3000 rpm (lilac waveforms in the bottom panel).

Preprints (www.preprints.org) | NOT PEER-REVIEWED | Posted: 20 October 2022 doi:10.20944/preprints202210.0314.v1

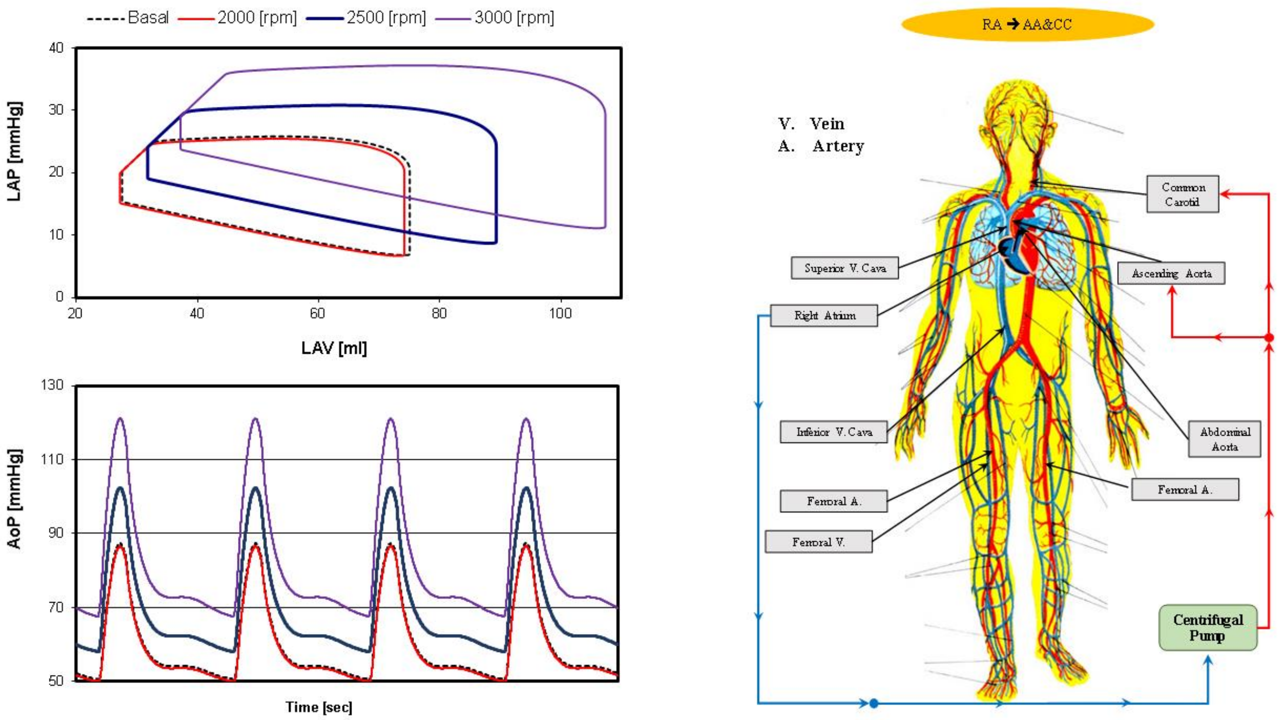

Figure 7. Left atrial pressure-volume loops (top left panel) and instantaneous AoP waveforms (bottom left panel) obtained in basal conditions (black dashed line) and with RA➔AA&CC cannulation when the pump rotational speed was set to 2000 (red line), 2500 (blue line) and 3000 (lilac line) rpm. The ventricular loops and the instantaneous waveforms obtained using CARDIOSIM© were stored in excel files and subsequently plotted. In RA➔AA&CC cannulation (right panel) the centrifugal pump draws blood from the right atrium and ejects it in the ascending aorta and common carotid artery bilaterally.

Figure 8 shows the initial analysis of percentage variation of AoP, CO, left (right) atrial pressure LAP (RAP) for the four different cannulation strategies compared to basal conditions when the rotational pump speed was set to 2500 rpm. Percentage variation of mean AoP, CO and LAP decreased for RA➔FA&CC and FV&SVC➔FA&CC cannulations. A decrease in percentage variation of the right atrial pressure was observed for FV&SVC➔FA&CC cannulation (bottom right panel).

Figure 9 shows the relative changes of cardiac output calculated in comparison to basal conditions for the four methods of cannulation. The simulations were performed setting pump rotational speed to 2000, 2500, 3000, 3500, 4000 and 4500 rpm. In the case of RA➔AA&CC (FV➔FA&CC) cannulation, CO increased up to 58% (52%) when the pump speed was set to 4500 rpm (top left panel and bottom right panel). On the contrary, in the case of RA➔FA&CC cannulation CO decreased by 17% when the pump speed was set to 4500 rpm (upper right panel).

Preprints (www.preprints.org) | NOT PEER-REVIEWED | Posted: 20 October 2022 doi:10.20944/preprints202210.0314.v1

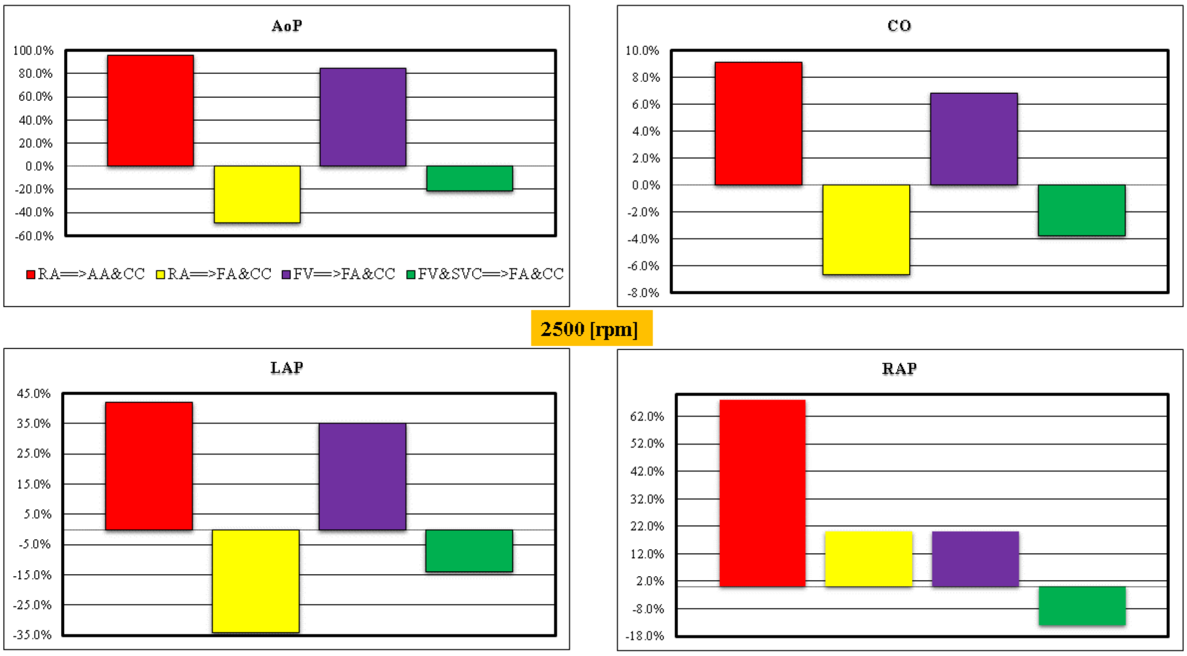

Figure 8. Relative changes calculated in comparison to basal conditions for the four different methods of cannulation with a pump rotational speed set to 2500 rpm. The top (bottom) left panel shows the relative changes in the aortic pressure AoP (left atrial pressure). The top (bottom) right panel shows the relative changes in the cardiac output CO (right atrial pressure).

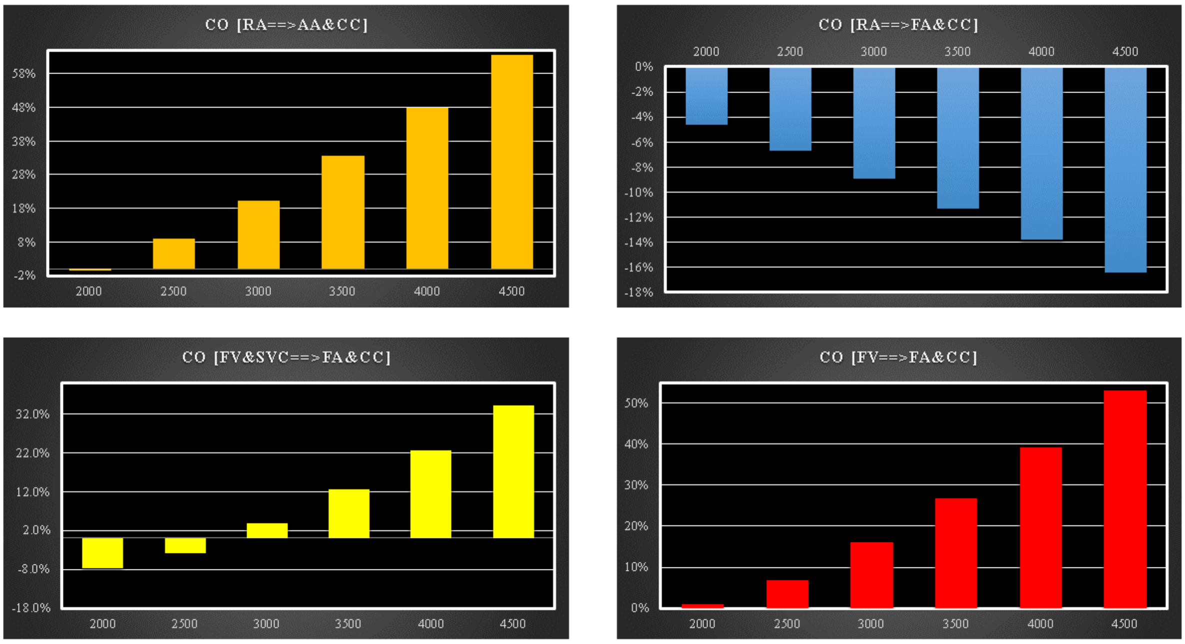

Figure 9. Relative CO changes calculated in comparison to basal conditions for the four different cannulation strategy at different pump rotational speed. The top (bottom) left panel shows the relative changes in CO induced by RA➔AA&CC (FV&SVC➔FA&CC) cannulation. The top (bottom) right panel shows the relative changes in cardiac output induced by RA➔FA&CC (FV➔FA&CC) cannulation.

Preprints (www.preprints.org) | NOT PEER-REVIEWED | Posted: 20 October 2022 doi:10.20944/preprints202210.0314.v1

For FV&SVC➔FA&CC cannulation, the outcome of the simulations showed that cardiac output took a positive turn when the rotational pump speed was set to 3000 rpm (lower left panel). A percentage increase in excess of 32% (compared to the basal conditions) in CO was observed when the pump speed was set to 4500 rpm.

The analysis of the two parameters that measure the coupling between the circulatory arterial network and the two ventricles and of the left and right ventricular external work is summarized in Figure 10 for all the cannulations with pump rotational speed set to 3500 rpm.

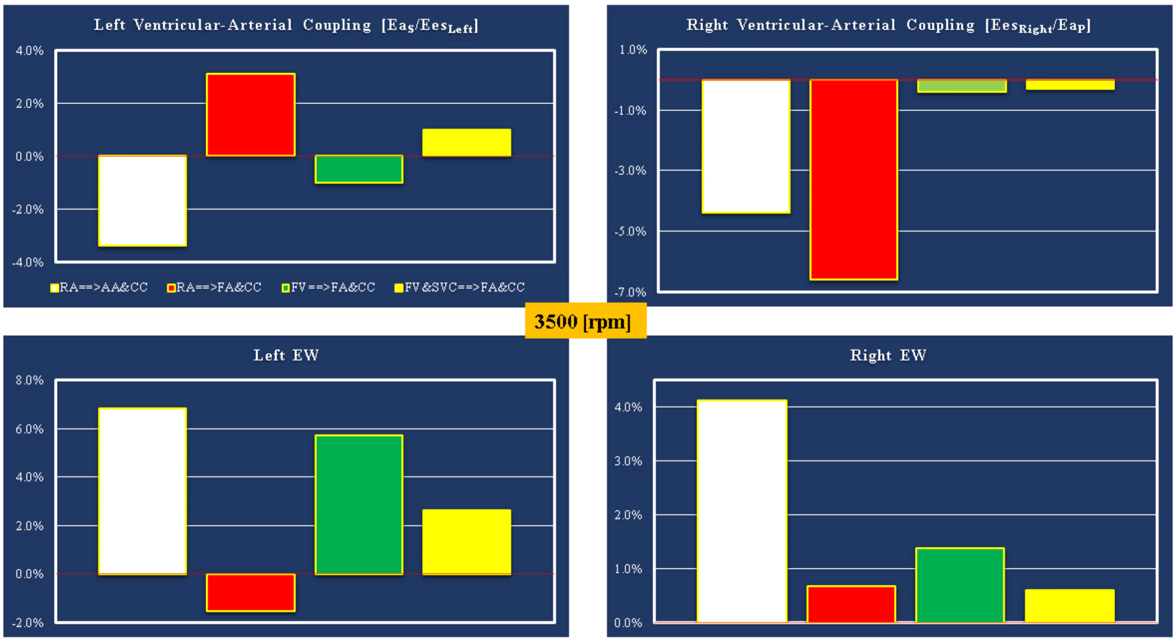

Figure 10. The top left (right) panel shows the relative changes of left (right) ventricular- arterial coupling Eas/EesLeft (EaP/EesRight) for different cannulations applied with pump rotational speed set to 3500 rpm. The relative changes estimate respect to basal conditions of the energetic variable (EW) for the left (right) ventricle is reported in the bottom left (right) panel.

An increase in Eas/EesLeft (top left panel) for both RA➔FA&CC and FV&SVC➔FA&CC cannulations was observed when pump rotational speed was set to 3500 rpm. On the contrary, the right ventricular-arterial coupling showed a percentage reduction compared to the basal values for all types of cannulation (top right panel). Only the RA➔FA&CC cannulation configuration underwent a reduction in left ventricular EW of less than 2%. EW increase up to 7% was observed for the RA➔AA&CC cannulation method (bottom left panel). When the pump speed was set to 3500 rpm, a modest percentage increase in right ventricular EW compared to baseline conditions (bottom right panel) was observed for all the cannulation configurations.

An analysis of the percentage changes in left ventricular EW (right ventricular PVA) for FV➔FA&CC, FV&SVC➔FA&CC and RA➔AA&CC cannulation configurations when the pump rotational speed was set to 2000, 2500, 3000, 3500, 4000 and 4500 rpm is shown in the top left (right) panel of Figure 11. When the pump speed was set to 4500 rpm, an increase of more than 15% in left ventricular EW and about 25% in right ventricular PVA was observed for the RA➔AA&CC cannulation configuration.

Preprints (www.preprints.org) | NOT PEER-REVIEWED | Posted: 20 October 2022 doi:10.20944/preprints202210.0314.v1

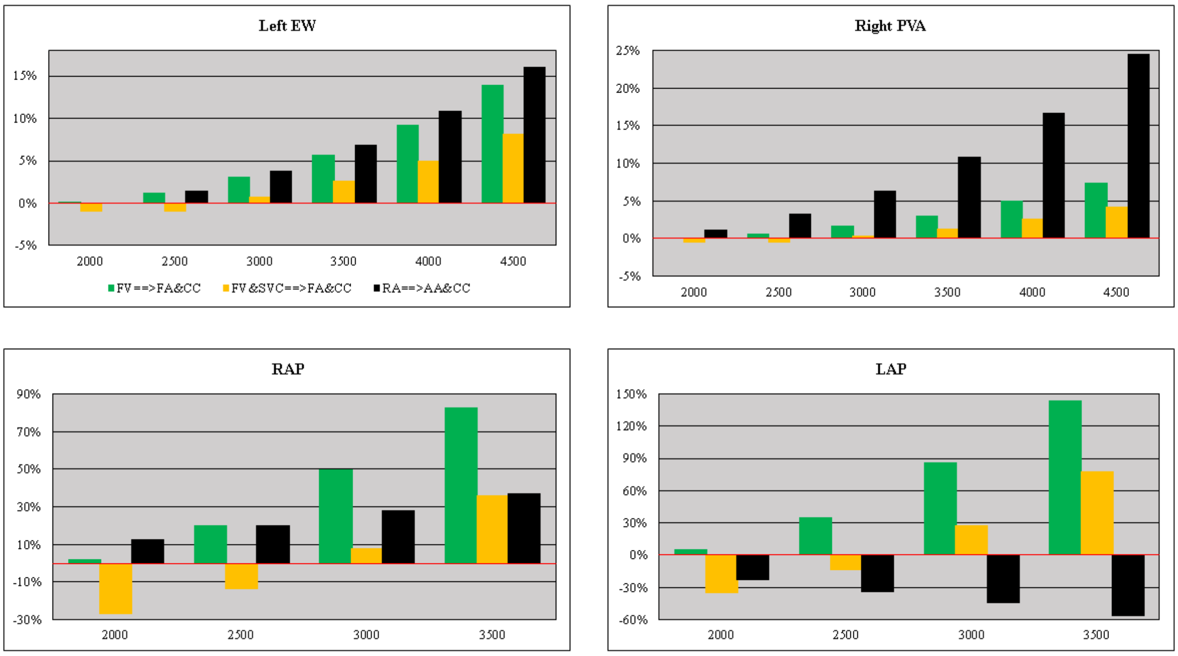

Figure 11. The top left (right) panel shows the relative changes in left (right) ventricular EW (PVA) observed for three different cannulations with pump rotational speed set to 2000, 2500, 3000, 3500, 4000 and 4500 rpm. The bottom left (right) panel shows the relative changes in right (left) atrial pressure compared to basal conditions for FV➔FA&CC, FV&SVC➔FA&CC and RA➔AA&CC cannulation configurations with pump rotational speed set to 2000, 2500, 3000 and 3500 rpm.

Percentage variation in RAP (LAP) compared to basal conditions are available in the bottom left (right) panel for FV➔FA&CC, FV&SVC➔FA&CC and RA➔AA&CC cannulation configurations simulated by setting the pump rotational speed to 2000, 2500 3000 and 3500 rpm. A percentage reduction in LAP (bottom right panel) is observed for RA➔AA&CC cannulation with each pump rotational speed.

Figure 12 shows the effects induced by the four different cannulation strategies on cerebral blood flow when the pump rotational speed was set to 3500 rpm (top left panel). The top right panel shows the effect induced by RA➔FA&CC cannulation on cerebral blood flow, superior vena cava flow and CO when the pump speed was set to 2500 rpm. The relative changes in cerebral blood flow*, SVC* and CO* have been evaluated when a little increase in the resistance of the ascending aorta tract was simulated.

Preprints (www.preprints.org) | NOT PEER-REVIEWED | Posted: 20 October 2022 doi:10.20944/preprints202210.0314.v1

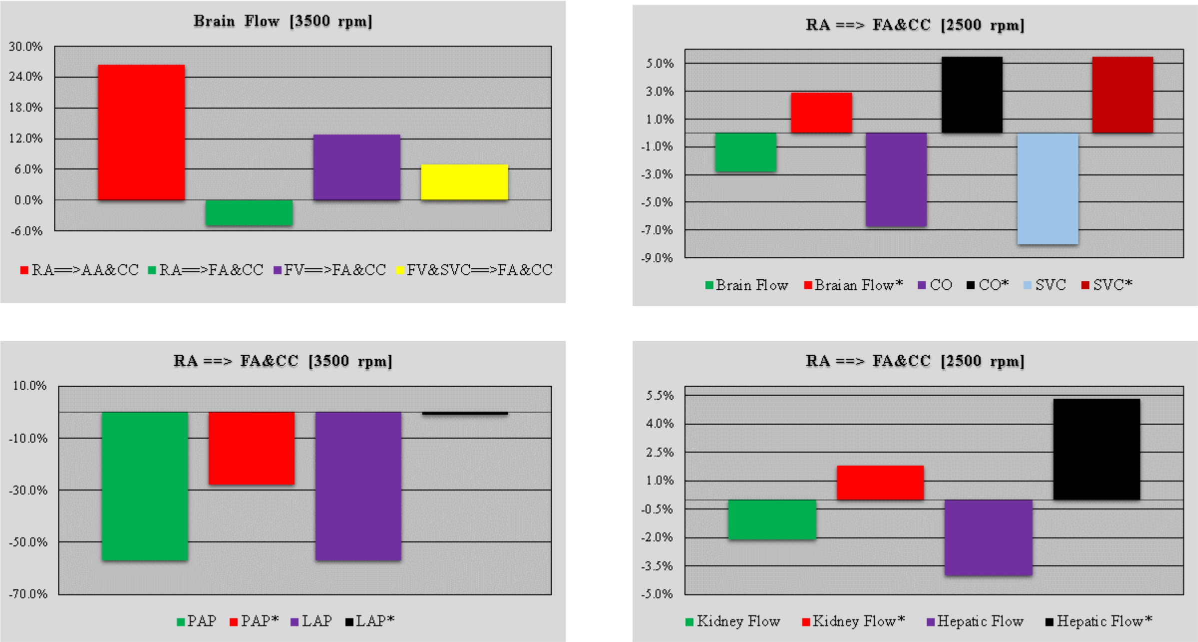

Figure 12. The top left panel shows the relative changes in cerebral blood flow induced by three different cannulation configurations with pump rotational speed set to 3500 rpm. The relative changes in cerebral blood flow, superior vena cava flow and cardiac output for RA➔FA&CC cannulation with pump speed set to 2500 rpm are available in the top right panel. Relative changes in CO*, cerebral blood flow* and SVC* blood flow have been evaluated when a little increase in ascending aorta resistance was considered during the simulation. Kidney flow*, hepatic flow* (bottom right panel), PAP* and LAP* (bottom left panel) have been evaluated in the same conditions when the pump rotational speed was set to 2500 and 3500 rpm, respectively.

The effects induced by the RA➔FA&CC cannulation strategy on PAP and LAP (kidney and hepatic flow) with pump rotational speed set to 3500 (2500) rpm are shown in the bottom left (right) panel. Percentage variation in kidney flow*, hepatic flow* (bottom right panel), PAP* and LAP* (bottom left panel) have been evaluated when a little increase in ascending aorta resistance was considered during the simulation.

The effects induced by different cannulation strategies on SVC and hepatic flow have been further analysed. Figure 13 shows the relative changes in SVC (top left panel) and hepatic flow (bottom left panel) obtained when the rotational pump speed was set to 3500 rpm. A percentage decrease was observed during RA➔FA&CC cannulation configuration. The top (bottom) right panel shows the relative changes in cerebral (kidney, hepatic and SVC) blood flow obtained when the FV&SVC➔FA&CC cannulation method was simulated with different rotational pump speeds. A trend reversal is observed when the pump speed is greater than or equal to 3000 rpm.

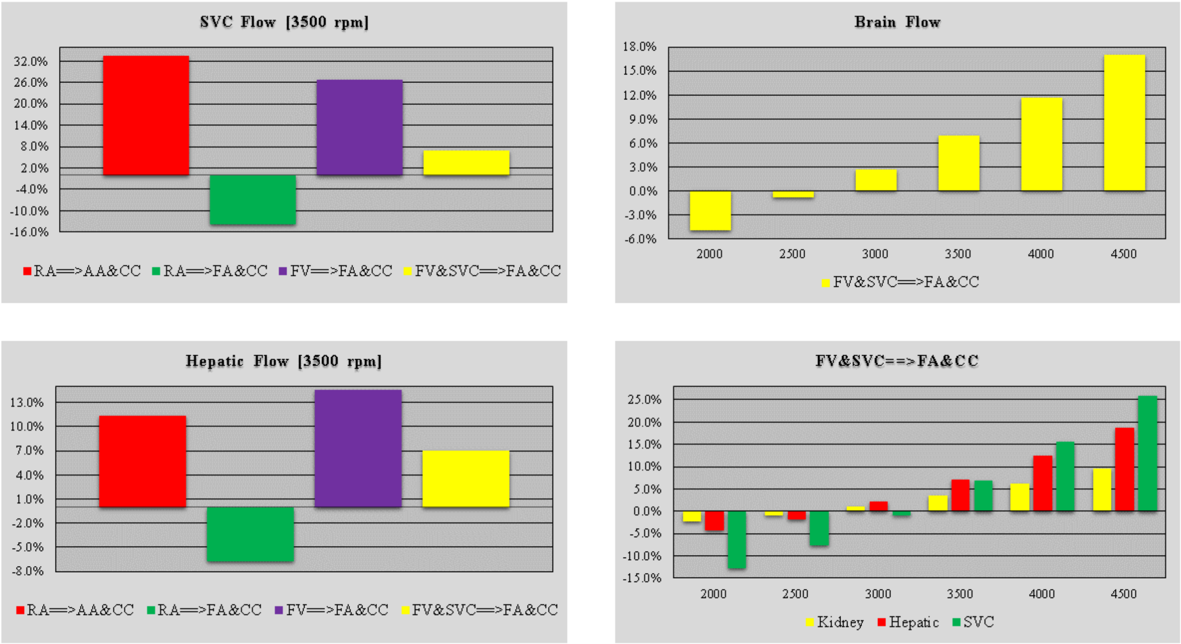

Figure 13. The top (bottom) left panel shows the relative changes in SVC flow (hepatic flow) induced by four different cannulation strategies obtained when the pump rotational speed was set to 3500 rpm. The top (bottom) right panel shows the cerebral flow (kidney, hepatic and SVC flow) for FV&SVC➔FA&CC cannulation method when the pump rotational speed was set to 2000, 2500, 3000, 3500 4000 and 4500 rpm.

4. Discussion

The management of aortic arch disease either in the context of acute type A aortic dissection or in the presence of aneurysmatic disease is quite challenging and still a matter of significant debate [49], [50]. Open repair for aortic arch disease remains the standard of care in high volume centres, although endovascular treatment has become quite an established approach in the presence of significant comorbidities [51]. Protection of cerebral blood flow remains the key issue during aortic arch replacement. RA➔AA&CC and FV➔FA&CC cannulation configurations increase and maintain cerebral perfusion appropriately up to 27% and 14% (Figure 12) confirming their adaptability according to the clinical setting. RA➔AA&CC cannulation would be quite appropriate for an elective aortic arch replacement due to severe aneurysmatic dilatation whilst FV➔FA&CC would be more appropriate in the presence of significant haematoma and dissection involving the whole aortic arch. An additional arterial cannula can be added before commencement of cardiopulmonary bypass to restore antegrade flow through the side branch of the Dacron graft after completion of the distal anastomosis during reconstruction of the aortic arch. RA➔FA&CC and FV&SVC➔FA&CC are suitable alternative but more dependent on pump setting and flow conditions (Figure 9 and 13). RA➔AA&CC and FV➔FA&CC cannulation configurations increase cardiac output up to 58% and 52% (Figure 8 and 9). The two cannulation configurations are consistent with increased cardiac output following stepwise increase in pump rotational speed The PV-loop analysis shows appropriate unloading of the left ventricle whilst the right ventricle seems less affected (Figure 4). This would be addressed by suction as required in routine cardiac surgery. FV&SVC➔FA&CC is consistent with increased cardiac output when pump rotational speed is at least 3000 rpm or above. Progressive decrease in cardiac output is observed with stepwise increase in pump rotational speed following RA➔FA&CC cannulation configuration.

Preprints (www.preprints.org) | NOT PEER-REVIEWED | Posted: 20 October 2022 doi:10.20944/preprints202210.0314.v1

5. Conclusion

The outcome of the simulations supports the successful set up of the three-way cannulation approach observed in clinical practice for aortic arch surgery with particular reference to RA➔AA&CC and FV➔FA&CC cannulation configurations. A close co-operation between cardiac surgeons, vascular surgeons and interventional radiologists remains essential to address aspects that are not completely within the domain of individual specialists. The contribution of engineering scientists may add a different dimension to clinical problem-solving.

Author Contributions: Conceptualization, C.DeL., B.DeL.; methodology, B.DeL.; software, C.DeL.; validation, C.DeL., B.DeL., M.C.; formal analysis, B.DeL.; investigation, C.DeL.; resources, C.DeL., M.C.; data curation, B.DeL.; writing—original draft preparation, C.DeL.; writing—review and editing, M.C., C.DeL., M.C., R.B.; visualization, B.DeL.; supervision, C.DeL., M.C.; project administration, C.DeL.; analysis of clinical and literature data, R.B., M.C. All authors have read and agreed to the published version of the manuscript.

Funding: This research received no external funding.

Institutional Review Board Statement: Not applicable.

Informed Consent Statement: Not applicable.

Data Availability Statement: Not applicable.

Acknowledgments: Not applicable.

Conflicts of Interest: The authors declare no conflict of interest.

References

1. Bachet, J. Open repair techniques in the aortic arch are still superior. *Ann. Cardiothorac. Surg.* **2018**, *7*, 328–344.
2. Chakos, A.; Jbara, D.; Yan, T.D.; Tian, D.H. Long-term survival and related outcomes for hybrid versus traditional arch repair—A meta-analysis. *Ann. Cardiothorac. Surg.* **2018**, *7*, 319–327.
3. Borst, H.G.; Walterbusch, G.; Schaps, D. Extensive aortic replacement using “elephant trunk” prosthesis. *Thorac. Cardiovasc. Surg.* **1983**, *31*, 37–40.
4. Schepens, M.A.; Dossche, K.M.; Morshuis, W.J.; van den Barselaar, P.J.; Heijmen, R.H.; Vermeulen, F.E. The elephant trunk technique: Operative results in 100 consecutive patients. *Eur. J. Cardiothorac. Surg.* **2002**, *21*, 276–281.
5. Shrestha M, Martens A, Krüger H; et al. Total aortic arch replacement with the elephant trunk technique: Single-centre 30-year results. *Eur. J. Cardiothorac. Surg.* **2014**, *45*, 289–296.
6. Karck, M.; Chavan, A.; Hagl, C.; Friedrich, H.; Galanski, M.; Haverich, A. The frozen elephant trunk technique: A new treatment for thoracic aortic aneurysms. *J. Thorac. Cardiovasc. Surg.* **2003**, *125*, 1550–1553.
7. Shrestha, M.; Bachet, J.; Bavaria, J.; Carrel, T.P.; De Paulis, R.; di Bartolomeo, R.; Etz, C.D.; Grabenwöger, M.; Grimm, M.; Haverich, A.; et al.Current status and recommendations for use of the frozen elephant trunk technique: A position paper by the Vascular Domain of EACTS. *Eur. J. Cardiothorac. Surg.* **2015**, *47*, 759–769.
8. De Bakey, M.E.; Crawford, E.S.; Cooley, D.A.; Morris, G.C., Jr. Successful resection of fusiform aneurysm of aortic arch with replacement by homograft. *Surg. Gynecol. Obstet.* **1957**, *105*, 657–664.
9. De Bakey, M.E.; Beall ACJr Cooley, D.A.; Crawford, E.S.; Morris, G.C., Jr.; Garrett, H.E. Resection and graft replacement of aneurysms involving the transverse arch of the aorta. *Surg. Clin. N. Am.* **1966**, *46*, 1057–1071.
10. Gega, A.; Rizzo, J.A.; Johnson, M.H.; Tranquilli, M.; Farkas, E.A.; Elefteriades, J.A. Straight Deep Hypothermic Arrest: Experience in 394 Patients Supports Its Effectiveness as a Sole Means of Brain Preservation. *Ann. Thorac. Surg.* **2007**, *84*, 759–767.
11. Ehrlich, M.P.; McCullough, J.N.; Zhang, N.; Weisz, D.J.; Juvonen, T.; A Bodian, C.; Griepp, R.B. Effect of Hypothermia on Cerebral Blood Flow and Metabolism in the Pig. *Ann. Thorac. Surg.* **2002**, *73*, 191–197.
12. Ueda, Y.; Miki, S.; Kusuhara, K.; Okita, Y.; Tahata, T.; Yamanaka, K. Deep Hypothermic Systemic Circulatory Arrest and Continuous Retrograde Cerebral Perfusion for Surgery of Aortic Arch Aneurysm. *Eur. J. Cardiothorac. Surg.* **1992**, *6*, 36–41; discussion 42.

Preprints (www.preprints.org) | NOT PEER-REVIEWED | Posted: 20 October 2022 doi:10.20944/preprints202210.0314.v1

13. Boeckxstaens, C.J.; Flameng, W.J. Retrograde Cerebral Perfusion Does Not Perfuse the Brain in Nonhuman Primates. *Ann. Thorac. Surg.* **1995**, *60*, 319–328.
14. de Brux, J.L.; Subayi, J.B.; Pegis, J.D.; Pillet, J. Retrograde Cerebral Perfusion: Anatomic Study of the Distribution of Blood to the Brain. *Ann. Thorac. Surg.* **1995**, *60*, 1294–1298.
15. Reich, D.L.; Uysal, S.; Ergin, M.A.; Griepp, R.B. Retrograde Cerebral Perfusion as a Method of Neuroprotection during Thoracic Aortic Surgery. *Ann Thorac. Surg.* **2001**, *72*, 1774–1782.
16. Ehrlich, M.P.; Hagl, C.; McCullough, J.N.; Zhang, N.; Shiang, H.; Bodian, C.; Griepp, R.B. Retrograde cerebral perfusion provides negligible flow through brain capillaries in the pig. *J. Thorac. Cardiovasc. Surg.* **2001**, *122*, 331–338.
17. Künzli, A.; Zingg, P.O.; Zünd, G.; Leskosek, B.; von Segesser, L.K. Does retrograde cerebral perfusion via superior vena cava cannulation protect the brain? *Eur. J. Cardiothorac. Surg.* **2006**, *30*, 906–909.
18. Estrera, A.L.; Miller, I.I.I.C.C.; Lee, T.Y.; Shah, P.; Safi, H.J. Ascending and transverse aortic arch repair: The impact of retrograde cerebral perfusion. *Circulation* **2008**, *118*, S160–S166.
19. Lau, C.; Gaudino, M.; Iannacone, E.M.; Gambardella, I.; Munjal, M.; Ohmes, L.B.; Degner, B.C.; Girardi, L.N. Retrograde cerebral Perfusion is Effective for Prolonged Circulatory Arrest in Arch Aneurysm Repair. *Ann. Thorac. Surg.* **2018**, *105*, 491–497.
20. Kazui, T.; Inoue, N.; Yamada, O.; Komatsu, S. Selective Cerebral Perfusion During Operation for Aneurysms of the Aortic Arch: A Reassessment. *Ann. Thorac. Surg.* **1992**, *53*, 109–114.
21. Kazui, T.; Yamashita, K.; Washiyama, N.; Terada, H.; Bashar, A.H.M.; Suzuki, T.; Ohkura, K.Usefulness of Antegrade Selective Cerebral Perfusion during Aortic Arch Operations. *Ann. Thorac. Surg.* **2002**, *74*, S1806–S1809.
22. Kazui, T. Total arch replacement with separated graft technique and selective antegrade cerebral perfusion. *Ann. Cardiothorac. Surg.* **2013**, *2*, 353–357.
23. Bachet, J.; Guilmet, D.; Goudot, B.; Termignon, J.L.; Teodori, G.; Dreyfus, G.; Brodaty, D.; Dubois, C.; Delentdecker, P.; Cabrol, C. Cold cerebroplegia. A new technique of cerebral protection during operations on the transverse aortic arch. *J. Thorac Cardiovasc. Surg.* **1991**, *102*, 85–94.
24. Bachet, J.; Guilmet, D.; Goudot, B.; Dreyfus, G.D.; Delentdecker, P.; Brodaty, D.; Dubois, C. Antegrade Cerebral Perfusion with Cold Blood: A 13-Year Experience. *Ann. Thorac. Surg.* **1999**, *67*, 1874–1878.
25. Pacini, D.; Leone, A.; Di Marco, L.; Marsilli, D.; Sobaih, F.; Turci, S.; Masieri, V.; Di Bartolomeo, R. Antegrade selective cerebral perfusion in thoracic aorta surgery: Safety of moderate hypothermia. *Eur. J. Cardiothorac. Surg.* **2007**, *31*, 618–622.
26. Salazar, J.; Coleman, R.; Griffith, S.; McNeil, J.; Young, H.; Calhoon, J.; Serrano, F.; DiGeronimo, R. Brain preservation with selective cerebral perfusion for operations requiring circulatory arrest: Protection at 25 °C is similar to 18 °C with shorter operating times. *Eur. J. Cardiothorac. Surg.* **2009**, *36*, 524–531.
27. Küçüker, S.A.; Özatik, M.A.; Saritaş, A.; Taşdemir, O. Arch repair with unilateral antegrade cerebral perfusion. *Eur. J. Cardiothorac. Surg.* **2005**, *27*, 638–643.
28. Malvindi, P.G.; Scrascia, G.; Vitale, N. Is unilateral antegrade cerebral perfusion equivalent to bilateral cerebral perfusion for patients undergoing aortic arch surgery? *Interact. Cardiovasc Thorac. Surg.* **2008**, *7*, 891–897.
29. Krähenbühl, E.S.; Reineke, D.; Aymard, T.; Clément, M.; Czerny, M.; Stalder, M.; Schmidli, J.; Carrel, T. Antegrade cerebral protection in thoracic aortic surgery: Lessons from the past decade. *Eur. J. Cardiothorac. Surg.* **2010**, *38*, 46–51.
30. Urbanski, P.P.; Lenos, A.; Blume, J.C.; Ziegler, V.; Griewing, B.; Schmitt, R.; Diegeler, A.; Dinkel, M. Does anatomical completeness of the circle of Willis correlate with sufficient cross-perfusion during unilateral cerebral perfusion? *Eur. J. Cardiothorac. Surg.* **2008**, *33*, 402–408.
31. Matalanis, G.; Koirala, R.S.; Shi, W.Y.; Hayward, P.A.; McCall, P.R. Branch-first aortic arch replacement with no circulatory arrest or deep hypothermia. *J. Thorac. Cardiovasc. Surg.* **2011**, *142*, 809–815.
32. Matalanis, G.; Ip, S. Total aortic repair for acute type a aortic dissection: A new paradigm. *J. Vis. Surg.* **2018**, *4*, 79.
33. Sabik, J.F.; Lytle, B.W.; McCarthy, P.M.; Cosgrove, D.M. Axillary artery: An alternative site of arterial cannulation for patients with extensive aortic and peripheral vascular disease. *J. Thorac. Cardiovasc. Surg.* **1995**, *109*, 885–890; discussion 890–891.
34. Schachner, T.; Nagiller, J.; Zimmer, A.; Laufer, G.; Bonatti, J. Technical problems and complications of axillary artery cannulation. *Eur. J. Cardiothorac. Surg.* **2005**, *27*, 634–637.

Preprints (www.preprints.org) | NOT PEER-REVIEWED | Posted: 20 October 2022 doi:10.20944/preprints202210.0314.v1

35. Di Eusanio, M.; Ciano, M.; Labriola, G.; Lionetti, G.; Di Eusanio, G. Cannulation of the innominate artery during surgery of the thoracic aorta: Our experience in 55 patients. *Eur. J. Cardiothorac. Surg.* **2007**, *32*, 270–273.
36. Urbanski, P.P.; Lenos, A.; Lindemann, Y.; Weigang, E.; Zacher, M.; Diegeler, A. Carotid artery cannulation in aortic surgery. *J. Thorac. Cardiovasc. Surg.* **2006**, *132*, 1398–1403.
37. Capoccia M, Nienaber CA, Mireskandari M, Sabetai M, Young C, Cheshire NJ, Rosendahl UP. Alternative Approach for Cerebral Protection during Complex Aortic Arch and Redo Surgery. *J. Cardiovasc. Dev. Dis.* **2021**, 8, 86.
38. De Lazzari, C.; Stalteri, D. 2011-2019, CARDIOSIM© Website. Original website platform regarding the implementation of the cardiovascular software simulator CARDIOSIM©. (https://cardiosim.dsb.cnr.it/).
39. De Lazzari, C.; et al. Interactive simulator for e-Learning environments: a teaching software for health care professionals, *BioMed. Eng. OnLine*. **2014**, 13, 172.
40. De Lazzari, C. Interaction between the septum and the left (right) ventricular free wall in order to evaluate the effects on coronary blood flow: numerical simulation. *Comput. Methods Biomech. Biomed. Eng*. **2012**, *15(12)*, 1359-1368.
41. De Lazzari, B.; Iacovoni, A.; Capoccia, M.; Papa, S.; Badagliacca, R.; Filomena, D.; De Lazzari, C. Ventricular and Atrial Pressure—Volume Loops: Analysis of the Effects Induced by Right Centrifugal Pump Assistance, *Bioengineering*. **2022**, 9(5), 181.
42. Capoccia, M.; Marconi, S.; Singh, S.A.; et al. Simulation as a preoperative planning approach in advanced heart failure patients. A retrospective clinical analysis. *BioMed. Eng. OnLine*. **2018**, *17(1)*, 52.
43. De Lazzari, B.; Iacovoni, A.; Mottaghy, K.; Capoccia, M.; Badagliacca, R.; Vizza C.D.; and De Lazzari, C. ECMO Assistance During Mechanical Ventilation: Effects Induced on Energetic and Haemodynamic Variables. *Comput. Methods. Programs. Biomed.* **2021**, *202*, 1-13.
44. De Lazzari, C.; De Lazzari, B.; Iacovoni, A.; Marconi, S.; Papa, S.; Capoccia, M.; Badagliacca, R.; Vizza, C.D. Intra-Aortic Balloon Counterpulsation Timing: A New Numerical Model for Programming and Training in the Clinical Environment. *Comput. Methods. Programs. Biomed*. 2020, 194, 1-9.
45. De Lazzari, C.; Stalteri, D. 2011–2019, CARDIOSIM© Website. Available online: https://cardiosim.dsb.cnr.it/CirculationModels/ncm2 (accessed on 6 April 2022).
46. Capoccia, M.; Marconi, S.; and De Lazzari, C. Decision-making in advanced heart failure patients requiring LVAD insertion: Can preoperative simulation become the way forward? A case study. *J. Biomed. Eng. Informatics.* **2018**, *4(2)*, 8-20. https://doi.org/10.5430/jbei.v4n2p (accessed on 6 April 2022).
47. De Lazzari, C.; Stalteri, D. 2011-2019, CARDIOSIM© Website. https://cardiosim.dsb.cnr.it/CirculationModels/pci4 (accessed on 6 April 2022).
48. De Lazzari, C; Stalteri, D. 2011-2019, CARDIOSIM© Website. https://cardiosim.dsb.cnr.it/AssistDevices/ecmo (accessed on 6 April 2022).
49. Safi, H.J.; Miller, I.I.I.C.C.; Estrera, A.L.; Villa, M.A.; Goodrick, J.S.; Porat, E.; Azizzadeh, A. Optimization of Aortic Arch Replacement: Two-Stage Approach. *Ann. Thorac. Surg.* **2007**, *83*, S815–S818.
50. Leone, A.; Di Marco, L.; Murana, G.; Coppola, G.; Fiorentino, M.F.; Amodio, C.; Di Bartolomeo, R.; Pacini, D. The Decision-Making Process in Acute Type a Aortic Dissection: When to Replace the Aortic Arch. *Semin. Thorac. Cardiovasc. Surg.* **2019**, *31*, 691–696.
51. Czerny, M.; Schmidli, J.; Adler, S.; Van Den Berg, J.C.; Bertoglio, L.; Carrel, T.; Chiesa, R.; Clough, R.E.; Eberle, B.; Etz, C.; et al. Editor's Choice—Current Options and Recommendations for the Treatment of Thoracic Aortic Pathologies Involving the Aortic Arch: An Expert Consensus Document of the European Association for Cardio-Thoracic Surgery (EACTS) & the European Society for Vascular Surgery (ESVS). *Eur. J. Vasc. Endovasc. Surg.* **2019**, *57*, 165–198.